SPE 100512

Injectivity Impairment due to Sulphate Scaling during PWRI: Analytical Model

P.G. Bedrikovetsky, SPE, North Fluminense State University (LENEP/UENF); E.J. Mackay, SPE, Heriot-Watt University; R.P. Monteiro and F. Patricio, North Fluminense State University (LENEP/UENF); F.F. Rosário, Petrobras/CENPES

Abstract

Previous work has derived an analytical model for simultaneous flow of incompatible waters in porous media with sulphate salt precipitation, determined typical values of the kinetics reaction coefficient from corefloods and what the impact would be on productivity impairment during sulphate scaling.

This paper extends the previous work, by modelling the injectivity impairment during simultaneous injection of incompatible waters, i.e. cation-rich produced water (PWRI) and seawater with sulphate anions. An analytical model with explicit expressions for deposited concentration and injectivity decline was developed.

The location of scale deposition and the resulting injectivity impairment are calculated for a range of sensitivities, including reaction kinetics (ranging from minimum to maximum values as obtained from coreflood and field data), fraction of produced water in the injected mixture and barium concentration in produced/re-injected water.

The theoretical parameter of the size of formation-damaged zone was introduced. It was found that almost all deposition takes place in a neighbourhood occupying a distance 2-4 times the well radius.

Calculations show that simultaneous injection of seawater with produced water containing even decimal fractions of ppm of barium would results in significant injectivity decline.

Introduction

Sulphate scaling with consequent deposit formation and wellbore damage is a well-known phenomenon that occurs during waterflooding, when mixing of incompatible injection and formation waters may result in sulphate salt precipitation and flow restriction[1]. The most significant damage occurs in and near production wells, where dispersion and chemical kinetics are particularly high due to high fluid velocities, and where the mixing of the different brines is most pronounced[2]. Sulphate scaling productivity impairment has been widely reported for North Sea, Gulf of Mexico and Persian Gulf fields[3,4].

Produced water re-injection (PWRI) involves injection of some additional water in order to fulfil the injection-production volumetric balance. In offshore waterflood projects, PWRI is complemented by seawater injection. The produced water may contain barium, strontium, magnesium and other metal cations, as well as seawater that is sulphate-rich. Simultaneous injection of incompatible waters results in sulphate salt deposition and consequent injectivity impairment[5].

The injectivity decline depends on the metal cation concentration in the injected water, the formation damage coefficient, the kinetics of chemical reaction and of salt deposition, the rock permeability and the injection rate. The

injectivity prediction and consequent decision making on PWRI, on mixing with seawater and on scale inhibition/removal requires laboratory-based mathematical modelling[5].

Mathematical modelling and laboratory studies of sulphate scaling are widely available in the literature[6-17].

The mathematical model for reactive flow consists of mass balances for all species that account for chemical reactions and hydrodynamic dispersion[8,12,17-18].

Axi symmetric diffusion-free equations of multiple chemical reactions during injection can be solved analytically using method of characteristics[19]. The same applies for quasi steady state production of injected and formation waters with sulphate scaling and productivity impairment[20]; the analytical model shows that the skin factor is proportional to the volume of produced water.

The dispersion-free model contains two empirical parameters: the kinetics coefficient characterizing the chemical reaction velocity, and the formation damage coefficient reflecting the permeability decline due to salt precipitation[16,17]. Both coefficients can be determined from either coreflood or production well history. The kinetics coefficient as a kinematics parameter can be determined from core effluent concentration (from concentration in produced water in production well case)[21]. The formation damage coefficient as a dynamics parameter can be determined from the increase of the pressure drop on the core (productivity index decrease). Both inverse problems are well posed[21].

This paper discusses injectivity impairment due to sulphate scaling during commingled injection of seawater and produced waters. Irreversibility of the scaling chemical reaction is assumed, and symmetric radial flow is assumed to take place around the injector in a reservoir. An analytical model based on exact solutions of the flow equations and incorporating the chemical reaction is developed. The main result is a linear dependency of the reciprocal injectivity index with time, with the most significant damage occurring within a radius equivalent to 2-4 times the wellbore radius. The proportionality coefficient (a so-called impedance slope) determines the injectivity decline during PWRI.

The maximum barium concentration in the injected brine that may be tolerated before significant injectivity decline has order of magnitude of 0.01-0.1 ppm. Thus, particular care must be taken with produced water composition when used for PWRI simultaneously with seawater.

Mathematical Model for PWRI Near-Well Sulphate Scaling

The injectivity impairment during simultaneous injection of produced water and seawater occurs due to chemical reaction between sulphate anions in the seawater and barium / strontium cations in the produced water. The reaction product – barium sulphate salt – deposits on the rock causing permeability reduction and consequent injectivity decline.

The schema of sulphate scaling during PWRI is presented in **Fig.1**. The accumulation of precipitant occurs near to the injector wellbore.

The mathematical model for sulphate scaling during simultaneous injection of two incompatible waters is given by a system of four equations, eqs. A-1[8,12,17].

One phase flow of aqueous solution with Ba^{2+} and SO_4^{2-} ions is assumed to occur in the presence of residual oil. Water and rock are assumed to be incompressible.

The Amagat law for overall volume balance of reacting fluid and precipitating solids holds. It results in conservation of water flux[22,23]. Therefore, water flux Q in eqs. A-1 depends on time only and in the considered particular case is assumed to be constant.

The first and second eqs. A-1 are mass balances for barium cations and sulphate anions, respectively. The equations account for second order chemical reaction between two species; law of acting masses[24-30] determines the chemical reaction rate on the right hand side of mass balance equations.

The chemical reaction rate constant K_a in porous media is also flow-velocity-dependent[30]. Following experimental data[16,17] we assume proportionality between the chemical reaction rate constant K_a and flow velocity, eqs. A-2. The proportionality coefficient λ is called the kinetics constant; its dimension is $(M*m)^{-1}$. The kinetics constant λ is equal to the reciprocal to the reference distance that one mole of reagent moves in order to almost completely disappear due to chemical reaction.

The model, eqs. A-1, also accounts for hydrodynamic dispersion of species in water flux; the dispersion coefficient is assumed to be proportional to flow velocity U, eqs. A-3[22,31]. The proportionality coefficient–the dispersivity α_D–is equal to the reference size of rock micro heterogeneity that causes the mixing.

The third eq. A-1 is mass balance for solid deposit that precipitates due to the chemical reaction.

Darcy's law, fourth eq. A-1, accounts for permeability reduction due to solid precipitant. Following, the hyperbolic dependence of permeability on deposited concentration was chosen[32]. The permeability reduction in this case is determined by one constant - the formation damage coefficient β.

The model, eqs. A-1, consists of four equations for four unknowns c_{Ba}, c_{SO4}, σ and p. The first two equations, eqs. A-1, are independent of σ and p, so they may be considered separately from the third and fourth equations.

The model, eqs. A-1, describes the reacting flow during simultaneous produced water re-injection and seawater injection in offshore oilfields undergoing waterflooding.

The introduction of dimensionless parameters, eqs. A-4, transfers system, eqs. A-1 to A-3, to dimensional form, eqs. A-5. At this point we assume instant mixing of two simultaneously injected waters in the reservoir and ignore species dispersion, eqs. A-6.

The bulk of precipitant accumulates near to the wellbore; the size of the affected zone is equal to several well radii. Therefore, the well radius is selected as a reference size of the sulphate scaling injectivity reduction process and is used to dimensionalise radial co-ordinate r at axi symmetric flow, eqs. A-4.

Barium and sulphate concentrations are dimensionalized by their concentrations in the injected water, c^0_{Ba} and c^0_{SO4} respectively.

Seawater and produced water are mixed in proportion N:1. For a given barium concentration in produced water c^1_{Ba} and sulphate concentration in seawater c^1_{SO4}, barium and sulphate concentrations in injected water are:

$$c^0_{Ba} = \frac{C^1_{Ba}}{N+1}, c^0_{SO_4} = \frac{N\,C^1_{SO_4}}{N+1} \quad \text{.....(1)}$$

The dimensionless system, eqs. A-5, contains three dimensionless parameters: ε_k, ε_D and α.

The chemical kinetics number ε_k is a ratio between well radius and the reference distance that one mole of reagent moves in order to almost disappear due to chemical reaction. Calculations based on **Table 1** shows that the chemical kinetics number ε_k varies in the range 0.6 to 50.

The diffusion number ε_D is the reciprocal to the Peclet number; it is equal to the ratio between dispersivity α_D and well radius r_w.

The concentration ratio α is the ratio between injected concentrations of barium and sulphate.

For simplicity, we ignore dispersion in mass balance equations for both ions, eqs. A-6.

Initial conditions, eqs. A-7, for PWRI sulphate scaling correspond to the absence of barium from the formation water at the beginning of re-injection. Initial sulphate concentration in the reservoir is equal to sulphate concentration in previously injected seawater.

Boundary conditions, eqs. A-8, correspond to fixing both concentrations c^0_{Ba} and c^0_{SO4} at the injector.

Analytical Model for Sulphate Scaling in Well Vicinity

The analytical solution of the problem of simultaneous injection of two incompatible waters, eqs. A-6 to A-8, is found in Appendix B by the method of characteristics[19].

Fig. 2 shows the structure of the flow zone. The front of the injected water displaces through the reservoir with dimensionless speed $(1-s_{or})^{-1}$. Both species concentrations are equal to their initial values ahead of the injected water front.

Concentrations of both ions are steady state behind the front and are given by eq. B-9 and eq. B-10. **Fig. 3** presents barium concentration profiles for different values of the kinetics numbers for the case where the injected sulphate concentration highly exceeds that of barium, α=0.02.

The deposit concentration is given by eq. B-11. **Fig. 4a** shows the deposition profiles and how the deposit accumulates with time.

The ion concentrations are steady state behind the front while the deposit accumulates proportionally to time, eq. B-13, Fig. 2. The ion concentrations decrease with distance from unity at the well to

$$C(t_D) = \frac{(1-\alpha)\exp\left[-\varepsilon_k(1-\alpha)\left(\sqrt{x_{Dw}+\frac{t_D}{1-s_{or}}}-\sqrt{x_{Dw}}\right)\right]}{1-\alpha\exp\left[-\varepsilon_k(1-\alpha)\left(\sqrt{x_{Dw}+\frac{t_D}{1-s_{or}}}-\sqrt{x_{Dw}}\right)\right]} \quad \text{.....(2)}$$

at the front. The frontal concentration decreases exponentially with time tending to zero as time tends to infinity. The expression for the frontal concentration is obtained from eq. B-9 for barium concentration profile behind the injected water front.

The deposit concentration decreases from

$$S(x_{Dw}, t_D) = \frac{\varepsilon_k t_D}{2\sqrt{x_{Dw}}(1-s_{or})} \quad \text{.....(3)}$$

at the well to zero at the front. The expression for the deposited concentration at the well is obtained from eq. B-11 for the barium sulphate concentration profile.

Equation B-11 shows the dynamics of the precipitant profile at negligibly small times, until the concentration front

reaches the boundary of the formation damage zone, and at large times also. Soon after the beginning of produced water re-injection, the volume of injected water greatly exceeds the volume of formation the damage zone, and the precipitant concentration becomes proportional to time, eq. B-13. The precipitant concentration is

$$\sigma(x_D,t_D)=S_u(x_D)\frac{M_{BaSO_4}c_{Ba}^0 t_D}{2(1-s_{or})\rho_{BaSO_4}},$$
$$S_u(x_D)=\frac{\varepsilon_k C(x_D)\,Y(x_D)}{\sqrt{x_D}} \quad \text{.....(4)}$$

Therefore, the deposition profile is characterised by the function of x_D—$S_u(x_D)$. The plots for different kinetics numbers and concentration ratios are presented in **Fig. 4b**.

The explicit formulae for both reagents and deposited concentrations, eqs. B-9, B-10 and B-13, allow derivation of the explicit formula for injectivity index versus time. Following[32], let us introduce impedance, which is the reciprocal to the dimensionless injectivity index

$$J(t_D)=\frac{II(0)}{II(t_D)}=\frac{\Delta P(t_D)q(0)}{\Delta P(0)q(t_D)} \quad \text{.....(5)}$$

While the injectivity index decreases, the impedance increases.

The main result of the injectivity index derivations from Appendix C is proportionality between the impedance and time:

$$J(t_D)=1+mt_D$$
$$m=\frac{\beta c_{Ba}^0}{2(1-s_{or})\ln\left(\frac{R_c}{r_w}\right)^2}\frac{M_{BaSO_4}}{\rho_{BaSO_4}}M(\varepsilon_k,\alpha) \quad \text{.....(6)}$$
$$M(\varepsilon_k,\alpha)=\varepsilon_k\int_1^{x_{Dd}}\frac{C(x_D)Y(x_D)}{x_D\sqrt{x_D}}dx_D$$

Here x_{Dd} is the size of the damaged zone, Appendix D. Barium sulphate deposition outside this zone does not affect injectivity; therefore the upper limit of integration in eqs. 6 is equal to x_{Dd}.

The impedance slope m depends on two empirical coefficients ε_k and β that characterise the sulphate scaling system, i.e. the porous medium and the fluid. The impedance slope is proportional to the formation damage coefficient β. Therefore, it is convenient to separate m into two coefficients: the first coefficient containing β and the impedance constant M; coefficient M depends on ε_k and is independent of β.

From eqs. 6 follows that skin factor is proportional to number of pore volumes injected (p.v.i.):

$$S_f=\frac{m}{2}\ln\left(\frac{R_c}{r_w}\right)t_D \quad \text{.....(7)}$$

Radius of Formation Damage Zone

The analytical solution shows that the precipitation area is the total space between the injected water front and the injector, Fig. 2. Nevertheless, the profiles for deposited salt, eq. B-13 abruptly decrease from the well towards the reservoir, Fig. 4. The greater the distance from the well to the point at which permeability is declining, the lower the impact on injectivity. The precipitation that affects well injectivity takes place in a zone around the injector 1.3 - 2.0 times the well radius. Let us define the formation damage zone radius r_d in such a way that the effect on well injectivity of the salt deposited in the reservoir at points far away from the well $r>r_d$ may be neglected.

The damaged zone radius is defined in Appendix D as a minimum radius of a zone outside which the deposited precipitant almost does not affect well injectivity, i.e. removal

of precipitant from the well neighbourhood with radius r_d would restore injectivity up to the level $1-\delta$ of its initial undamaged value J=1:

$$\int_1^{x_{Dd}} \frac{C(x_D)Y(x_D)}{x_D\sqrt{x_D}}dx_D = (1-\delta)\int_1^{x_{Dc}} \frac{C(x_D)Y(x_D)}{x_D\sqrt{x_D}}dx_D \quad \text{.....(8)}$$

The precision of δ depends on the precision of the reservoir simulation in each particular case; it could be 0.01, 0.1, etc.

Fig. 5 shows the plot of impedance constant $M(x_D)$ versus contour radius for the real field case (reservoir A, North Sea): reservoir thickness h= 152.4 m, half-distance from injector to producer R_c= 500 m; well radius r_w= 0.15 m; sulphate concentration in injected water $c_{SO4}{}^0$= 3000 ppm; porosity ϕ= 0.18; rate Q= 55000 bbl/day. The impedance constant M for this case is given by curve 1. Here we use λ= 4000 $(M*m)^{-1}$, where M is molar unit for concentration one *gmol/L* (the same as $kgmol/m^3$).

Curves 2, 3 and 4 differ from the real case by values of ε_k and α. Curve 1 almost coincides with curve 2, as well as curve 3 almost coincides with curve 4. So, for small values of concentration ratio α, the value of α only slightly affects the impedance constant M.

Let us explain the phenomenon of independence of the impedance constant M of the concentration ratio α for cases of small concentration ratio, α<<1. When the barium concentration is negligible (much lower than that of sulphate), the chemical reaction does not cause a significant reduction in the sulphate concentration. Asymptotic expansion of barium profile, eq. B-9, over small α results in zero-order term, so the barium profile, eq. B-9, is proportional to the injected barium concentration. Fixing constant sulphate concentration in eq. B-13 we obtain proportionality between impedance constant m and c^0_{Ba}, eqs. C-8. The impedance constant M becomes independent of the concentration ratio α.

In Fig. 5 we used small α values, α<<1, so curves 1 and 2, 3 and 4 almost coincide.

Function $M(x_D)$ differs from its asymptotic value by 0.01 at x_{Dd}= 1.8 for ε_k= 18.74, which corresponds to r_d= 1.3 r_w. For ε_k= 4.7, $M(x_D)$ differs from its asymptotic value by 0.01 at x_{Dd}= 4.8, which is equal to 2.2 r_w. The formation damage zone size is therefore equal to only several well radii.

Fig. 6 shows dimensionless size of formation damage zone x_{Dd} versus kinetics number for two values of concentration ratio–0.02 and 0.2. The higher the kinetics number the faster precipitation occurs and the smaller is the zone of deposit accumulation. For cases where sulphate concentration highly exceeds barium concentration, the formation damage zone radius is almost independent of the barium concentration in the injected fluid.

Fig. 6 illustrates that the concentration radio almost does not affect the impedance slope – curves with α= 0.2 and 0.02 coincide.

Since the formation damage zone radius is usually equal to several well radii, in the present work we use the well radius r_w to adimentionalise the radial coordinate r, eqs. A-4. Therefore, dimensionless time is measured in injected fluid volumes, where the unit corresponds to

$$V_1 = \pi r_w^2 h\phi \quad \text{.....(9)}$$

which has order of magnitude of 1 cubic meter per meter of reservoir thickness.

The fact that a damaged zone has a size of several well radii is very important for well stimulation design. For example, the definition of the necessary volume of acid or solvent[33] to remove the scale is determined by the r_d value.

The formation damage zone volume is

$$V_d = \pi\left(r_d^2 - r_w^2\right)h\phi \quad \text{.....(10)}$$

which has order of magnitude of ten cubic meters per meter of reservoir thickness.

Formula 10 can be used for volume estimates of scaling removing solvent or of acidizing fluid. Using exact eq. 10 is particularly important for horizontal injectors where length may be hundred times higher than that for vertical wells, and consequently huge solvent/acid volumes may be required.

If additional perforation is planned in order to restore the injectivity, the perforation depth should exceed the radius of damaged zone.

Precipitation Profiles

Let us calculate the range variation of dimensionless kinetics number ε_k. The kinetics coefficient varies from 200 to 10000 $(M*m)^{-1}$ (see Table 1). Well radius r_w= 0.1 to 0.15 m, and sulphate concentration in seawater is generally close to 0.03 Molar (3000 ppm).

Fig. 3 shows the effect of kinetics number on barium concentration profile. As mentioned before, the profile is steady state behind the concentration front. Curves 1, 2, 3 and 4 correspond to different kinetics numbers - ε_k= 0.62, 3.12, 12.48 and 31.2 respectively. The above-mentioned kinetics number values correspond to the following values for kinetics coefficient: λ= 200, 1000, 4000 and 10000 $(M*m)^{-1}$ respectively. The concentration ratio is α = 0.02.

The higher kinetics number, the more intensive is the chemical reaction, and the more abrupt is barium concentration decline with radius.

Table 1 shows that the most typical kinetics coefficient values are λ= 1000 and 4000 $(M*m)^{-1}$, so the typical concentration profiles are presented by curves 2 and 3. Fig. 3 shows that despite the barium concentration being non-zero in the overall zone behind the injected water front, it almost disappears at the distance 1.4 to 2.5 well radii.

The precipitation profiles are shown in Fig. 4a for different dimensionless times: t_D= $5\cdot10^5$; 10^6; $5\cdot10^6$; $1.1\cdot10^7$ and ε_k= 18.72 (λ= 4000 $(M*m)^{-1}$). The maximum time t_D= $1.1\cdot10^7$ corresponds to one pore volume injected when the reservoir contour radius is 500 m. Deposit accumulates mainly near to the wellbore. Precipitation takes place in the well vicinity x_{Dd}= $1.6x_{Dw}$ that corresponds to damaged zone radius 1.28 r_w.

For the purposes of injectivity forecast we use times $t_D >> x_{Dd}$, where the injected water volume highly exceeds the damaged zone volume, and the precipitated concentration is proportional to time, eq. B-13. Therefore, the precipitation profile can be expressed by the function

$$S_u\left(x_D\right) = \frac{\varepsilon_k C\left(x_D\right) Y\left(x_D\right)}{\sqrt{x_D}}$$
$$S\left(x_D, t_D\right) = \frac{S_u\left(x_D\right) t_D}{2\left(1 - s_{or}\right)} \quad \text{.....(11)}$$

Fig. 4b presents S_u profile for different kinetics numbers and concentration ratios. The kinetics numbers are ε_k = 3.7 and

18.72 (λ = 800 and 4000 respectively) and concentration ratios are α = 0.01 and 0.1.

The higher is the kinetics number the higher is the precipitant concentration. Curves 3 and 4 lay above curves 1 and 2.

The dimensionless precipitation profile is almost independent of the concentration ratio α. Here we used small α values, α<<1, so barium concentration is much smaller than that of sulphate. In this case, as explained above, the solution $\sigma(x_D,t_D)$ is proportional to the injected barium concentration $c_{\mathrm{Ba}}{}^0$, and the dimensionless function $S(x_D,t_D)$ is independent of the concentration ratio α. Therefore, curves 1 and 2, 3 and 4 in Fig. 4b almost coincide. The concentration ratio α does not affect the profile $S_u(x_D)$ for small barium concentrations.

The profile $S_u(x_D)$ determines impedance slope M; see eqs. 6 and 11. Therefore, curves 1 and 2, 3 and 4 in Fig. 5, that differ from each other by α-value only, almost coincide.

The damaged zone radius is determined by $M(x_D)$ plots. Therefore, the concentration ratio α does not significantly influence the damaged zone size x_{Dd} for small α values, α<<1, Fig. 6.

Injectivity Index Calculations

The injectivity decline is characterised by impedance constant M, eq. 6. The slope depends on kinetics number and on concentration ratio. **Fig. 7a** presents the increase of M versus kinetics number for concentration ratios α= 0.01, 0.05, 0.1 and 1.0 (curves 1,2,3 and 4 respectively). The M-curves almost coincide for small concentration ratios α<0.1. It was explained above by a small variation of sulphate concentration where the governing system is linear and the solution is proportional to injected barium concentration. The M values slightly decrease for α = 1.

The higher is the kinetics number, the more intensive is the chemical reaction, so impedance constant M increases when ε_k increases. The constant M increases fast at small kinetics number values, where ε_k does not exceed 5 to 7; for large ε_k the slope tends to its asymptotic value. The impedance constant M is almost independent of the kinetics number for large ε_k values that exceed 20 to 30.

The dependency of the impedance constant M on concentration ratio is shown on **Fig. 7b** for kinetics numbers ε_k= 0.94, 4.68, 18.72 and 46.8. The above-mentioned small effect of α for α<0.1 and high effect of ε_k for ε_k < 10 can be seen from Fig. 7b also.

Time variation of well injectivity index and of impedance is shown in **Fig. 8** for concentration ratio α= 0.02. Impedance growth is shown in Fig. 8a; injectivity index decline is shown in Fig. 8b versus t_D in pore volumes injected, and in Fig. 8c – versus real time. The higher the kinetics number the faster are impedance growth and injectivity decline.

Changing Inlet Concentrations and fractions SW:PW

Fig. 9 shows how injectivity index declines for four different barium concentrations in injected water. The higher is the injected concentration the higher is the deposited concentration and the lower is the injectivity index. Here we calculated the real case of field A (North Sea, UK). The damaged zone radius was calculated by eq. D-1 – r_d = 0.4m.

The plots in Fig. 9a and 9b allows us to compare different ratios of mixed produced and sea waters during injection. The ratio seawater: produced water is *N:*1. Recalculation of injected barium concentration using eqs. 1 allows plotting injectivity decline versus fraction *N*. **Fig. 10** presents three cases of mixing the produced and sea-waters for c_{Ba}= 80 ppm in produced water; c_{SO4}= 2800 ppm in seawater. Here we took the most common value for kinetics coefficient λ= 4000 $(M*m)^{-1}$ that corresponds to ε_k= 13.92, α= 0.005; ε_k= 8.7, α= 0.02 and ε_k= 3.48, α= 0.08 for curves 1, 2 and 3 respectively. The lower is the seawater fraction, the lower is the sulphate concentration. For all cases, sulphate concentration greatly exceeds that for barium, so α<<1, and the solution is proportional to the injected barium concentration. The reaction rate is proportional to sulphate concentration. Therefore, the lower is the seawater fraction, the lower is the barium concentration decline. The location of curves 1, 2 and 3 in Fig. 10 confirms the conclusion.

Fig. 11 shows profiles for $S_u(x_D)$ and for deposition $S(x_D,t_D)$, t_D= 1 p.v.i., for the three above-mentioned cases. It is possible observe that the higher is the seawater fraction, the greater the deposition near to the well (continuous curve lies above two other curves in well vicinity). The impact of deposition on injectivity is most pronounced near to the well, it can be illustrated by the fact that $x_D^{3/2}$ appears in the denominator of the integrant in eq. C-6. Therefore, the case of high seawater fraction exposes the higher formation damage: curve 1 in plot $M(x_D)$ lays above two other curves.

Fig. 12 presents impedance constant *M* versus contour radius $x= x_{Dc}$. These plots allow us to calculate the formation damage zone radius r_d. The obtained r_d values are equal to several well radii. Maximum value r_d= 0.39 m was used in calculation of the impedance and the injectivity index for three above-mentioned cases of PWRI.

Effects of the ratio *N* of seawater to produced water on impedance constant *M* and on impedance slope *m* are shown in **Fig. 13 and Fig. 14**. Dependency of the impedance constant *M* on injected sulphate ion concentration is determined mainly by the term of ε_k in front of the integral, eqs. .6; the integral is almost independent of N since the solution is almost independent of concentration ration α for sulphate concentrations that highly exceed barium concentrations; ε_k is proportional to the injected sulphate ion concentration. Therefore, the impedance constant *M* increases with increase of the ratio *N*. For high *N* and excess of sulphate, *M* is determined by barium ion concentration and tends to constant value, **Fig. 13**.

The impedance slope *m* is low for the cases of high excess of either barium or sulphate. Therefore, *m* is small for large and small ratios *N*. It explains non-monotonic dependency of slope *m* on ratio *N,* **Fig. 14**.

Fig. 15a shows impedance versus pore volume of injected water t_D. Injectivity index decrease versus pore volume of injected water is presented in **Fig. 15b**. Injectivity index versus real time is shown in **Fig. 15c**. The higher the seawater fraction, the lower is the injectivity index.

Maximum Barium Concentration in Re-Injected Water

Formula 6 with correspondent plots from **Fig. 9 through 15**, allows us to calculate the maximum barium concentration in injected water causing a given injectivity index decline.

The data are presented in **Table 2a and 2b**. First column exposes the period of two times injectivity decrease in pore volume injected, the second column shows this period in real time, and the third column exposes the corresponding barium concentration.

Here we took the following data from offshore field A, North Sea, UK: reservoir thickness h= 152.4 m, half-distance from injector to producer R_c= 500 m; well radius r_w= 0.15 m; sulphate concentration in injected water c_{SO4}^0= 3000 ppm; porosity ϕ= 0.18; λ= 4000 (M*m)$^{-1}$; rate Q= 55000 bbl/day. **Table 2a** corresponds to the case of two times injectivity decrease during one pore volume injected, **Table 2b** shows barium concentration for five times decrease of injectivity.

PWRI using produced water with a barium concentration of 0.04 ppm results in two times decrease of injectivity after one p.v.i. If the barium concentration is equal to 0.159 ppm, the injectivity after one p.v.i. decreases five times.

Fig. 16 shows dependencies of maximum barium concentration on kinetics constant λ and on kinetics number ε_k. The more intensive is the chemical reaction, the higher is the formation damage for a given barium concentration. Therefore, maximum barium concentration decreases when the kinetics number increases.

During one p.v.i., the number of injected pore volumes of damaged zone is $(R_c/r_d)^2$ - that is approximately $4*10^6$. During simultaneous steady-state flow of two reagents through a rock during millions of p.v.i., even a very small concentration of one of the reagents may cause significant permeability damage.

Characterisation of Sulphate Scaling System from Injectivity Data

The reactive flow model, eqs. A-5, for simultaneous injection of seawater and produced water with consequent injectivity damage contains three independent physics constants: concentration ratio α, kinetics coefficient λ and formation damage coefficient β. The concentration ratio is known from the analysis of injected waters while the kinetics and formation damage coefficients are phenomenological parameters that characterise the rock-fluid system and cannot be predicted theoretically for real rocks and fluids. These two coefficients must be determined from either laboratory or well data. Nevertheless, just one constant can be determined from injectivity decline data, which is the impedance slope m.

Dependence of the impedance slope m on λ and β is given by eqs. 6. So, one equation for two unknowns is available for characterisation of the sulphate scaling system from injectivity decline data.

One of ways around the problem is using laboratory coreflood data on simultaneous flow of produced and sea waters. Outlet barium concentration allows us to calculate the kinetics coefficient λ, and pressure drop on the core determines the formation damage coefficient β[17]. Measurements of pressure in the middle of the core along with pressure at core edges substitutes the effluent concentration

information and allows us to calculate both λ and β (so called 3-point-pressure method[34,35]).

Another way around is using the pressure build up test for the injector. Wellbore pressure evolution during the test allows us to calculate the permeability profile around the well[36]. This leads to second equation

$$k(r) = \frac{k_0}{1+\beta\sigma\left(r, t_D^0\right)} \quad \text{.....(12)}$$

permitting calculation of both coefficients λ and β.

Discussions

The mathematical model for simultaneous injection of seawater and produced water with consequent injectivity damage depends on three dimensionless parameters: kinetics and formation damage coefficients and concentration ratio. The kinetics and formation damage coefficients are phenomenological parameters that characterise the rock-fluid system and cannot be predicted theoretically for real rocks and fluids. Two coefficients must be determined from either laboratory or well data.

An analytical model shows that during simultaneous injection of incompatible waters, the concentration front moves with the velocity of the injected water. Both reagent concentrations are zero ahead of this front and are steady state behind the front. The deposited concentration linearly increases with time.

The precipitant accumulates in each point of the reservoir after passing the point by the concentration front. The deposited concentration is proportional to injected water volume. The reciprocal to injectivity index is also proportional to injected water volume, and the proportionality coefficient (impedance slope) determines how fast the injectivity falls down. The impedance slope is proportional to formation damage coefficient. The impedance slope can be determined from the well injectivity decline data.

The accumulating deposit decreases the injectivity only inside a limited area around the injector; the deposit is small outside this area and does not affect injectivity. The area is determined by so called formation damage size. Calculations show that the formation damage size equals several well radii. This information is important for calculating the amount of damage removal fluid (solvent, acid), or for determining the perforation depth, or for interpretation of logging data.

If barium concentration in the injected mixture is significantly lower than that of sulphate, the deposited concentration and the impedance slope are proportional to the injected barium concentration. They are also proportional to the fraction of produced water in the injected mixture with seawater. These facts are important for planning the produced/injected water management/treatment, including decision making on mixing sea and produced waters, treatment of produced water, and frequency of scale removal operations.

If scale inhibitors are to be used to protect the injection infrastructure from scale damage, then these calculations indicate how far into the formation the inhibitor will have to penetrate to prevent significant damage. A separate calculation of inhibitor retardation due to adsorption may be performed to indicate the volume of chemical that will be required to protect the well.

Even 0.1 to 0.01 ppm concentrations of barium in produced water being re-injected simultaneously with seawater may cause significant injectivity damage. Therefore, it is very important to take care of the composition of produced water used for PWRI.

Conclusions

The analytical modelling of sulphate deposition during simultaneous injection of produced and sea waters allows us to make the following conclusions:

1. The system of simultaneous injection of two incompatible waters is fully defined by two empirical parameters: the formation damage coefficient and the kinetics number.
2. Despite the precipitation area being the total space between the injected water front and injector, the precipitation that affects well injectivity takes place in a zone 1.5 to 3.0 times the well radius from the injector.
3. The defined formation damage zone radius is an important characteristic of PWRI with simultaneous seawater injection, allowing calculation of the necessary acid volume in case of acidification, solvent volume in case of sulphate removal, or scale inhibitor volume in the case of inhibition.
4. The deposited concentration at each reservoir point is proportional to injected water volume.
5. The increase of reciprocal injectivity index (impedance) is proportional to injected water volume.
6. The impedance slope is proportional to formation damage coefficient and depends on kinetics number. The well injectivity decline data allows calculation either of two model parameters.
7. If the injected sulphate concentration highly exceeds the injected barium concentration, the deposition profile and impedance increase are proportional to the injected barium concentration. The dimensionless deposition profile and the damage zone size are independent of the concentration ratio α.
8. Simultaneous injection of seawater with produced water containing even decimal fractions of ppm of barium would results in significant injectivity decline.

Acknowledgement

Authors thank Dr. A. L. S. da Souza and Alexandre G. Sequeira (Petrobras), Prof. Themis Carageorgos (UENF-LENEP), Dr. Oleg Dinariev and Prof. A. D. Polianin (Russian Academy of Sciences) for fruitful discussions. Numerous discussions with Prof Y. Yortsos (USC, USA) on reactive flows are greatly appreciated.

Nomenclature

C – dimensionless Ba^{2+} concentration

c_{Ba} – Ba^{2+} molar concentration in aqueous solution, M

c_{SO4} – SO_4^{2-} molar concentration in aqueous solution, M

D – dispersion coefficient, m^2/s

h – thickness, m

II – injectivity index, $m^3/(s \cdot Pa)$

J – dimensionless impedance

k_0 – initial permeability, D

K_a – chemical reaction rate constant, $(M \cdot s)^{-1}$ (2^{nd} order reaction)

k_{rwor} – relative permeability for water in the presence of residual oil

m – slope of the impedance straight line versus t_D

M – impedance constant

M_{BaSO4} – molecular weight for Barium Sulphate equals 0.23339 Kg/mol

p – Pressure, Pa

P – dimensionless pressure

Q – total rate, m^3/s

r – radial co-ordinate, m

R_c – contour radius, m

r_w – well radius, m

r_d – damage radius, m

s_{or} – residual oil saturation

S – dimensionless $BaSO_4$ concentration

t – time, s

t_D – dimensionless time, p.v.i.

U – flow velocity, m/s

V – concentration difference

x_D – dimensionless coordinate

x_{Dw} – dimensionless well coordinate

x_{Dd} – dimensionless damage zone coordinate

Y – dimensionless SO_4 concentration

Greek letters

α – ratio between injected concentrations of Ba^{2+} and SO_4^{2-}

α_D – dispersion coefficient, m

β – formation damage coefficient

ε_D – dimensionless diffusive (Schmidt) number

ε_k – dimensionless chemical kinetics number

ϕ – porosity

λ – kinetics intensity, $(M \cdot m)^{-1}$ (2^{nd} order reaction)

μ_w – water viscosity, kg/(m·s)

ρ_{BaSO4} density of the Barite, 4193.9 Kg/m^3

σ – $BaSO_4$ molar concentration in solid deposit, M

References

1. Oddo, J.E. and Tomson, M.B.: "Why Scale Forms and How to Predict It," *SPEPF* (February 1994) 47–54.
2. Sorbie, K.S. and Mackay, E.J.: "Mixing of Injected, Connate and Aquifer Brines in Waterflooding and its Relevance to Oilfield Scaling," *Journal Petroleum Science and Engineering* (2000) **27**, 85–106.
3. Rosario, F. F. and Bezerra, M.C.: "Scale Potential of a Deep Water Field – Water Characterization and Scaling Assessment," paper SPE 68332 presented at the 2001 SPE Third International Symposium on Oilfield Scaling, Aberdeen, UK, 30–31 January.
4. Gomes, J. *et al.*: "The Impact of Mineral Scale Formation on Deep Water Fields: A Campos Basin Overview, SPE paper presented at the 2002 SPE Oilfield Scaling Symposium, Aberdeen, UK, 30–31 January.
5. Jordan, M.M., Collins, I.R. and Mackay, E.J.: "Low Sulfate Seawater Injection for Barium Sulfate Scale Control: A Life-of-Field Solution to a Complex Challenge," paper SPE 98096 presented at the 2006 SPE International Symposium and Exhibition on Formation Damage Control, Lafayette, L.A., 15–17 February.

6. Mackay, E.J. and Graham, G.M.: "The Use of Flow Models in Assessing the Risk of Scale Damage," paper SPE 80252 presented at the 2002 SPE International Symposium Oilfield Chemistry, Houston, Texas, USA, 20–21 February.
7. Mackay, E.J, Jordan, M.M. and Torabi, F.: "Predicting Brine Mixing Deep Within the Reservoir, and the Impact on Scale Control in Marginal and Deepwater Developments," paper SPE 73779 presented at the 2002 SPE International Symposium and Exhibition on Formation Damage Control, Lafayette, LA, 20–21 February.
8. Rocha, A. *et al*.: "Numerical Modelling of Salt Precipitation During Produced Water Reinjection," paper SPE 68336 presented at the 2001 SPE Third International Symposium on Oilfield Scaling, Aberdeen, UK, 30–31 January.
9. Mackay, E.J.: "Modelling of In-Situ Scale Deposition: The Impact of Reservoir and Well Geometries and Kinetics Reaction Rates," paper SPE 74683 presented at the 2002 SPE Oilfield Scaling Symposium, Aberdeen, UK, 30–31 January.
10. Daher, J. S. *et al*.: "Evaluation of Inorganic Scale Deposition in Unconsolidated Reservoir by Numerical Simulation," paper SPE 95107 presented at the 2005 SPE 7th International Symposium on Oilfield Scale, Aberdeen, UK, 11–12 May.
11. Delshad, M. and Pope, G.A.: "Effect of Dispersion on Transport and Precipitation of Barium and Sulphate in Oil Reservoir," paper SPE 80253 presented at the 2003 SPE International Symposium on Oilfield Chemistry, Houston, Texas, USA, 5–7 February.
12. Woods, A.W. and Parker, G.: "Barium Sulphate Precipitation in Porous Rock Through Dispersive Mixing," paper SPE 80401 presented at the 2003 SPE 5th International Symposium on Oilfield Scale, Aberdeen, UK, 29–30 January.
13. Allaga, D.A. *et al*.: "Barium and Calcium Sulphate Precipitation and Migration inside Sandpacks," *SPEFE* (March 1992).
14. Wat, R.M.S. *et al*.: "Kinetics of BaSO4 Crystal Growth and Effect in Formation Damage," paper SPE 23814 presented at the 1992 SPE International Symposium on Formation Damage Control, Lafayette, Louisiana, February 26–27.
15. Todd, A.C. and Yuan, M.D.: "Barium and Strontium Sulphate Solid-Solution Scale Formation at Elevated Temperatures," *SPEPE* (February 1992) 85–92.
16. Lopes Jr., R.P., "Barium Sulphate Kinetics of Precipitation in Porous Media: Mathematical and Laboratory Modelling," in Portuguese, MS Thesis, North Fluminense State University-Lenep/UENF, Macaé, RJ, Brazil (2002).
17. Bedrikovetsky, P.G. *et al*.: "Barium Sulphate Oilfield Scaling: Mathematical and Laboratory Modelling," paper SPE 87457 presented at the 2004 SPE 6th International Symposium on Oilfield Scale, Aberdeen, UK, May 26–27.
18. Green, D.W. and Willhite, G.P.: *Enhanced Oil Recovery,* Textbook Series, SPE, (1998).
19. Araque-Martinez, A. and Lake, L.W.: "A Simplified Approach to Geochemical Modelling and its Effect on Well Impairment," paper SPE 56678 presented at the 1999 SPE Annual Technical Conference and Exhibition, Houston, Texas, 3–6 October.
20. Bedrikovetsky, P.G. *et al*.: "Oilfield Scaling – Part II: Productivity Index Theory," paper SPE 81128 presented at the 2003 SPE Latin American and Caribbean Petroleum Engineering Conference, Port-of-Spain, Trinidad, West Indies, 27–30 April.
21. Alvarez, A.C. *et al*.: "A fast inverse solver for the filtration function for flow of water with particles in porous media," *Journal of Inverse Problems* (2006) v. v.22, 69–88.

22. Lake, L.W.: *Enhanced Oil Recovery*, Prentice Hall, Engelwood Cliffs, NY, (1989).
23. Bedrikovetsky, P.G.: *Mathematical Theory of Oil and Gas Recovery,* Kluwer Academic Publishers, London/Boston (1994).
24. Stumm, W.: *Chemistry of Solid-Water Interface,* John Wiley and Sons, New York City, (1992) 428.
25. Bethke, C.: *Geochemical Reaction Modelling,* Oxford University Press, (1996) 397.
26. Nielsen, A.E.: "The Kinetics of Crystal Growth in Barium Sulphate Precipitation II – Temperature Dependence and Mechanism," *Acta Chemical Scandinavica* (1959) 13, 784–802.
27. Schechter, R.A.: *Oil Well Stimulation,* Prentice Hall, Englewood Cliffs, New Jersey, (1992).
28. Nancollas, G. and Liu, T.: "Crystal Growth and Dissolution of Barium Sulphate", paper SPE 5300 presented at the 1975 SPE/AIME Oilfield Chemistry Symposium, Dallas, January.
29. Dunn, K., *et. al*.: "Mechanisms of Precipitation and Dissolution of Barite: A Morphology Approach," *Journal of Coll and Interface Science* (1991) **214**, 427–437.
30. Fogler, S.: *Chemical Reactions Engineering,* Prentice Hall, New York City, (1998).
31. Nikolaevskii, V.N.: *Mechanics of Porous and Fractured Media,* World Scientific Publishing Co., Singapure (1990).
32. Pang, S. and Sharma, M.M.: "A Model for Predicting Injectivity Decline in Water Injection Wells," paper SPE 28489 presented at the 1994 SPE 69th Annual Technical Conference and Exhibition, New Orleans, LA, September 25–28.
33. Lakatos István, Lakatos-Szabó Julianna: "Effect of pH on Solubility of Barium Sulfate in Presence of Different Polyamino Carboxylic Acids**,"** pp. 59-76 in LAKATOS I. (ed.) "Focus on Remaining Oil and Gas Reserves", Progress in Mining and Oilfield Chemistry, Vol. 4., Akadémiai Kiadó, Budapest (2002).
34. Bedrikovetsky P.G. *et al*.: "Characterization of Deep Bed Filtration System from Laboratory Pressure Drop Measurements," *Journal of Petroleum Science and Engineering* (2001) 64, No. 3, 167–177.
35. Bedrikovetsky, P.G. *et al*.: "Characterization of Deep Bed Filtration from Pressure Measurements," *SPEPF* (2003) No 3, 119–128.
36. Feitosa, G. S. *et al*.: "Determination of permeability distribution from well-test pressure data," *JPT* (July 1994) 607–614.

Appendix A. Governing Equations for Sulphate Scaling in Porous Media

The system of governing equations for axi symmetric flow of aqueous solution of barium and sulphate ions with precipitation of solid barium sulphate consists of mass balance equations for barium cations, for sulphate anions, for barium sulphate and of the modified Darcy's law accounting for permeability reduction due to solid salt deposition[8,12,17]:

$$
\begin{aligned}
&2\pi rh\phi\left(1-s_{\text{or}}\right)\frac{\partial c_{\text{Ba}}}{\partial t}+\frac{\partial}{\partial r}\left(Qc_{\text{Ba}}-2\pi rhD\frac{\partial c_{\text{Ba}}}{\partial r}\right)\\
&=-2\pi rhK_a c_{\text{Ba}}c_{\text{SO}_4}\\
&2\pi rh\phi\left(1-s_{\text{or}}\right)\frac{\partial c_{\text{SO}_4}}{\partial t}+\frac{\partial}{\partial r}\left(Qc_{\text{SO}_4}-2\pi rhD\frac{\partial c_{\text{SO}_4}}{\partial r}\right)\\
&=-2\pi rhK_a c_{\text{Ba}}c_{\text{SO}_4}\\
&\phi\left(1-s_{\text{or}}\right)\frac{\rho_{\text{BaSO}_4}}{M_{\text{BaSO}_4}}\frac{\partial\sigma}{\partial t}=K_a c_{\text{Ba}}c_{\text{SO}_4}\\
&U=\frac{Q}{2\pi rh}=-\frac{k_0 k_{rwor}}{\mu\left(1+\beta\sigma\right)}\frac{\partial p}{\partial r}
\end{aligned}
\qquad \text{.....(A-1)}
$$

According to numerous coreflood data, we assume that the chemical reaction rate constant K_a is proportional to flow velocity[16,17]

$$K_a = \lambda U \quad \text{.....(A-2)}$$

It is assumed that the dispersion coefficients for Ba^{2+} and SO_4^{2-} ions are equal and proportional to flow velocity[31]:

$$D_{\mathrm{Ba}} \cong D_{\mathrm{SO_4}} \cong D = \alpha_D U \quad \text{.....(A-3)}$$

Let us introduce the following dimensionless parameters:

$$C = \frac{c_{\mathrm{Ba}}}{c^0_{\mathrm{Ba}}},\ Y = \frac{c_{\mathrm{SO_4}}}{c^0_{\mathrm{SO_4}}},\ x_D = \left(\frac{r}{r_w}\right)^2,\ t_D = \frac{Qt}{\pi h \phi r_w^{\ 2}}$$

$$p_D = \frac{4\pi h k_0 k_{rwor} p}{\mu Q},\ S = \frac{\rho_{\mathrm{BaSO_4}}}{M_{\mathrm{BaSO_4}}}\frac{\sigma}{c^0_{\mathrm{Ba}}} \quad \text{.....(A-4)}$$

$$\varepsilon_D = \frac{\alpha_D}{r_w},\ \varepsilon_k = \lambda r_w c^0_{SO_4},\ \alpha = \frac{c^0_{\mathrm{Ba}}}{c^0_{\mathrm{SO_4}}}$$

Substituting dimensionless co-ordinates and parameters, eqs. A-4, in the system of governing, eqs. A-1, we obtain

$$\begin{aligned}
&(1 - s_{\mathrm{or}})\frac{\partial C}{\partial t_D} + \frac{\partial C}{\partial x_D} = \varepsilon_D \frac{\partial}{\partial x_D}\left(2\sqrt{x_D}\frac{\partial C}{\partial x_D}\right) - \frac{\varepsilon_k}{2\sqrt{x_D}} CY \\
&(1 - s_{\mathrm{or}})\frac{\partial Y}{\partial t_D} + \frac{\partial Y}{\partial x_D} = \varepsilon_D \frac{\partial}{\partial x_D}\left(2\sqrt{x_D}\frac{\partial Y}{\partial x_D}\right) - \frac{\varepsilon_k}{2\sqrt{x_D}} \alpha CY \\
&(1 - s_{\mathrm{or}})\frac{\partial S}{\partial t_D} = \frac{\varepsilon_k}{2\sqrt{x_D}} CY \\
&1 = -\frac{x_D}{\left(1 + \beta c^0_{\mathrm{Ba}} \frac{M_{\mathrm{BaSO_4}}}{\rho_{\mathrm{BaSO_4}}} S\right)} \frac{dp_D}{dx_D}
\end{aligned} \quad \text{(A-5)}$$

First two equations of A-5 are separated from the third and fourth equations. After neglecting the hydrodynamic dispersion, equations take the form

$$\begin{aligned}
&(1 - s_{\mathrm{or}})\frac{\partial C}{\partial t_D} + \frac{\partial C}{\partial x_D} = -\frac{\varepsilon_k}{2\sqrt{x_D}} CY \\
&(1 - s_{\mathrm{or}})\frac{\partial Y}{\partial t_D} + \frac{\partial Y}{\partial x_D} = -\frac{\varepsilon_k}{2\sqrt{x_D}} \alpha CY
\end{aligned} \quad \text{.....(A-6)}$$

Displacement of water with SO_4^{2-} anions by Ba^{2+}- and SO_4^{2-}-rich water is described by the following initial conditions:

$t_D = 0$: $C = 0$, $Y = Y_0$ .....(A-7)

The re-injection of water with SO_4^{2-} anions and Ba^{2+} cations into the reservoir, saturated by Ba^{2+}- rich water, corresponds to the inlet boundary conditions where concentrations are fixed for both species:

$x_D = x_{Dw}$: $C = 1$, $Y = 1$ .....(A-8)

Appendix B. Analytical Model for 1D Flow

Both concentrations are equal to their initial values in the zone ahead of the injected water front

$$C = 0, Y = Y_0, \quad (1 - s_{or})(x_D - x_{Dw}) > t_D > 0 \quad \text{.....(B-1)}$$

Let us transform eqs. A-6 to characteristic form behind the front[19]

$$\begin{aligned}
&\frac{dt_D}{dx_D} = (1 - s_{or}) \\
&\frac{dC}{dx_D} = -\frac{\varepsilon_k}{2\sqrt{x_D}} CY \\
&\frac{1}{\alpha}\frac{dY}{dx_D} = -\frac{\varepsilon_k}{2\sqrt{x_D}} CY
\end{aligned} \quad \text{.....(B-2)}$$

Introduce the following linear combination of two concentrations:

$$V(x_D) = C(x_D) - \frac{Y(x_D)}{\alpha} \quad \text{.....(B-3)}$$

Let us multiply third eq. B-2 by α and subtract the product from the second eq. B-2. It results in the following conservation equation for $V(x_D)$:

$$\frac{dV}{dx_D} = 0 \quad \text{.....(B-4)}$$

The inlet boundary condition for $V(x_D)$ follows from eqs. A-8:

$$x_D = x_{Dw}: \quad V = 1 - \frac{1}{\alpha} \quad \text{.....(B-5)}$$

As it follows from eq. B-4, V is constant, so

$$V = 1 - \frac{1}{\alpha} \quad \text{.....(B-6)}$$

So, the concentration difference, eq. B-3, is constant along the characteristics. Expressing the concentration Y versus x_D from eq. B-6.

$$Y(x_D) = 1 + \alpha\left[C(x_D) - 1\right] \quad \text{.....(B-7)}$$

and substituting it into second eq. B-2, we obtain an ordinary differential equation:

$$\frac{dC}{dx_D} = -\frac{\varepsilon_k}{2\sqrt{x_D}} C\left[1 + \alpha(C - 1)\right] \quad \text{.....(B-8)}$$

The first order ordinary differential equation, eq. B-8, with boundary condition, eqs. A-8, is solved by separation of variables:

$$C(x_D) = \frac{(1-\alpha)\exp\left[-\varepsilon_k (1-\alpha)\left(\sqrt{x_D} - \sqrt{x_{Dw}}\right)\right]}{1 - \alpha\exp\left[-\varepsilon_k (1-\alpha)\left(\sqrt{x_D} - \sqrt{x_{Dw}}\right)\right]} \quad \text{.....(B-9)}$$

Substituting solution, eq. B-9, into eq. B-7, we obtain sulphate concentration profile:

$$Y(x_D) = \alpha\left[\frac{(1-\alpha)\exp\left[-\varepsilon_k (1-\alpha)\left(\sqrt{x_D} - \sqrt{x_{Dw}}\right)\right]}{1 - \alpha\exp\left[-\varepsilon_k (1-\alpha)\left(\sqrt{x_D} - \sqrt{x_{Dw}}\right)\right]}\right] + 1 - \alpha \quad \text{.(B-10)}$$

The substitution of eq. B-9 and eq. B-10 into kinetics eqs. A-5 results in explicit formula for deposit accumulation:

$$S(x_D, t_D) = \frac{\varepsilon_k C(x_D)\, Y(x_D)}{2\sqrt{x_D}\,(1 - s_{or})}\left[t_D - \left[(1 - s_{or})(x_D - x_{Dw})\right]\right] \quad \text{...(B-11)}$$

For large times, when the injected water volume highly exceeds the damaged zone volume

$$t_D >> \left[(1 - s_{or})(x_{Dd} - x_{Dw})\right] \quad \text{.....(B-12)}$$

formula B-11 can be simplified

$$S(x_D, t_D) = \frac{\varepsilon_k C(x_D)\, Y(x_D)}{2\sqrt{x_D}\,(1 - s_{or})} t_D \quad \text{.....(B-13)}$$

The deposited concentration at large times is proportional to dimensionless time.

Appendix C. Injectivity Index Calculations

Let us calculate the pressure drop between the contour and the well using the pressure gradient expression as obtained from modified Darcy's law, fourth eq. A-1. The interval $[x_{D\,w}, x_{D\,c}]$ is divided into those of the damaged zone with alternated permeability $[x_{Dw}, x_{Dd}]$ and of the undamaged zone $[x_{Dd}, x_{Dc}]$:

$$\Delta P = \int_1^{x_{Dd}} -\frac{\partial P}{\partial x_D} dx_D + \int_{x_{Dd}}^{x_{Dc}} -\frac{\partial P}{\partial x_D} dx_D \quad \text{.....(C-1)}$$

Outside the damaged zone, the precipitant does not affect the injectivity. Deposited concentration at $x_D > x_{Dd}$ can be neglected.

Substituting pressure gradient from eqs. A-5 into eq. C-1, we obtain the following expression for pressure drop between injector and contour:

$$\Delta P = \ln\left(\frac{R_c}{r_w}\right)^2 + \beta c^0_{\mathrm{Ba}} \frac{M_{\mathrm{BaSO_4}}}{\rho_{\mathrm{BaSO_4}}} \int_1^{x_{Dd}} \frac{S(x_D, t_D)}{x_D} dx_D \quad \text{.....(C-2)}$$

Substituting dimensionless deposited concentration, eq. B-13 into eq. C-2, we obtain expression for the integral:

$$\int_1^{x_{Dd}} \frac{S(x_D)}{x_D} dx_D = \frac{\varepsilon_k t_D}{2(1 - s_{\mathrm{or}})} \int_1^{x_{Dd}} \frac{C(x_D) Y(x_D)}{x_D \sqrt{x_D}} dx_D \quad \text{.....(C-3)}$$

The final expression for the pressure drop is:

$$\Delta P = \ln\left(\frac{R_c}{r_w}\right)^2 + \frac{\beta \varepsilon_k c^0_{\mathrm{Ba}}}{2(1 - s_{\mathrm{or}})} \frac{M_{\mathrm{BaSO_4}}}{\rho_{\mathrm{BaSO_4}}} t_D \int_1^{x_{Dd}} \frac{C(x_D) Y(x_D)}{x_D \sqrt{x_D}} dx_D \quad \text{(C-4)}$$

Let us introduce the following dimensionless impedance function that is an inverse to dimensionless injectivity index

$$J(t_D) = \frac{Q^0}{\Delta P^0} \frac{\Delta P}{Q} \quad \text{.....(C-5)}$$

The impedance expression follows from eqs. C-4 and C-5

$$\frac{II^0}{II}(t_D) = 1 + \frac{\beta\varepsilon_k c_{\mathrm{Ba}}^0}{2(1-s_{or})\ln\left(\frac{R_c}{r_w}\right)^2}\frac{M_{\mathrm{BaSO_4}}}{\rho_{\mathrm{BaSO_4}}} T \int_1^{x_{Dd}} \frac{C(x_D)Y(x_D)}{x_D\sqrt{x_D}}dx_D \quad \text{(C-6)}$$

So, the impedance is a linear function of time

$$J(t_D) = 1 + mt_D$$

$$m = \frac{\beta\varepsilon_k c_{Ba}^0}{2(1-s_{or})\ln\left(\frac{R_c}{r_w}\right)^2}\frac{M_{\mathrm{BaSO_4}}}{\rho_{\mathrm{BaSO_4}}}\int_1^{x_{Dd}} \frac{C(x_D)Y(x_D)}{x_D\sqrt{x_D}}dx_D \quad \text{..(C-7)}$$

Taking constants off the impedance slope m, we introduce the impedance constant M:

$$m = \frac{\beta c_{Ba}^0}{2(1-s_{or})\ln\left(\frac{R_c}{r_w}\right)^2}\frac{M_{\mathrm{BaSO_4}}}{\rho_{\mathrm{BaSO_4}}}M$$

$$M(\varepsilon_k,\alpha) = \varepsilon_k \int_1^{x_{Dd}} \frac{C(x_D,\varepsilon_k,\alpha)Y(x_D,\varepsilon_k,\alpha)}{x_D\sqrt{x_D}}dx_D \quad \text{.....(C-8)}$$

Formula C-7 allows for determination of formation damage coefficient, β, from the pressure drop and injection rate data.

Appendix D. Radius of Formation Damage Zone

We choose the radius of formation damage zone r_d in such a way that pressure drop increase between the injection well $r=r_w$ and the damaged zone boundary $r=r_d$ is equal to 0.9 (0.99) of the total pressure drop increase between the injector and the contour $r=R_c$:

$$\int_{r_w}^{r_d} -\frac{\partial p}{\partial r}dr = (1-\delta)\int_{r_w}^{R_c} -\frac{\partial p}{\partial r}dr \quad \text{.....(D-1)}$$

Injectivity decline is determined by the slope m, eqs. C-7. So, the formation damage zone radius r_d is defined in terms of M: removal of deposition from the r_d well neighbourhood results in restoration of injectivity from its initial value $J = 1$ up to $J = 1-\delta$, i.e. incomplete removal is due to some deposit left outside the damaged zone

$$M(x_D,\varepsilon_k,\alpha) = \varepsilon_k \int_{x_{Dw}}^{x_D} \frac{C(x_D)Y(x_D)}{x_D\sqrt{x_D}}dx_D$$

$$\int_1^{x_{Dd}} \frac{C(x_D)Y(x_D)}{x_D\sqrt{x_D}}dx_D = (1-\delta)\int_1^{x_{Dc}} \frac{C(x_D)Y(x_D)}{x_D\sqrt{x_D}}dx_D \quad \text{.....(D-2)}$$

where the precision value δ could be taken as 0.01 or 0.1.

Let us calculate the integral in second eq. D-2. Opening the product of the concentrations inside the integral, we obtain:

$$M(x_D,\varepsilon_k,\alpha) = \varepsilon_k\alpha(1-\alpha)^2\int_{x_{Dw}}^{x_D}\frac{\exp\left[-2\varepsilon_k(1-\alpha)\left(\sqrt{x_D}-\sqrt{x_{Dw}}\right)\right]}{x_D\sqrt{x_D}\left[1-\alpha\exp\left[-\varepsilon_k(1-\alpha)\left(\sqrt{x_D}-\sqrt{x_{Dw}}\right)\right]\right]}dx_D$$

$$+\varepsilon_k\alpha(1-\alpha)^2\int_{x_{Dw}}^{x_D}\frac{\exp\left[-\varepsilon_k(1-\alpha)\left(\sqrt{x_D}-\sqrt{x_{Dw}}\right)\right]}{x_D\sqrt{x_D}\left[1-\alpha\exp\left[-\varepsilon_k(1-\alpha)\left(\sqrt{x_D}-\sqrt{x_{Dw}}\right)\right]\right]}dx_D \quad \text{.....(D-3)}$$

Calculate the integral of the first term in eq. D-3 using a new variable $u = \exp\left[-\varepsilon_k(1-\alpha)\sqrt{x_D}\right]$, instead of x_D:

$$\varepsilon_k\alpha(1-\alpha)^2\int_{x_{Dw}}^{x_D}\frac{\exp\left[-2\varepsilon_k(1-\alpha)\left(\sqrt{x_D}-\sqrt{x_{Dw}}\right)\right]}{x_D\sqrt{x_D}\left(1-\alpha\exp\left[-\varepsilon_k(1-\alpha)\left(\sqrt{x_D}-\sqrt{x_{Dw}}\right)\right]\right)^2}dx_D =$$

$$c_1\alpha\exp\left[\varepsilon_k(1-\alpha)\sqrt{x_{Dw}}\right]\int_{\exp\left[-\varepsilon_k(1-\alpha)\sqrt{x_{Dw}}\right]}^{\exp\left[-\varepsilon_k(1-\alpha)\sqrt{x_D}\right]}\frac{u}{(1-c_2u)^2\ln^2(u)}du \quad \text{...(D-4)}$$

The integral of the second term of eq. D-3 is:

$$\varepsilon_k(1-\alpha)^2\int_{x_{Dw}}^{x_D}\frac{\exp\left[-\varepsilon_k(1-\alpha)\left(\sqrt{x_D}-\sqrt{x_{Dw}}\right)\right]}{x_D\sqrt{x_D}\left(1-\alpha\exp\left[-\varepsilon_k(1-\alpha)\left(\sqrt{x_D}-\sqrt{x_{Dw}}\right)\right]\right)}dx_D =$$

$$c_1\int_{\exp\left(-\varepsilon_k(1-\alpha)\sqrt{x_{Dw}}\right)}^{\exp\left(-\varepsilon_k(1-\alpha)\sqrt{x_D}\right)}\frac{1}{(1-c_2u)\ln^2(u)}du \quad \text{.....(D-5)}$$

Eqs. D-4 and D-5 contain two constants:

$$c_1 = -2\varepsilon_k^{\,2}\left(1-\alpha\right)^3 \exp\left(\varepsilon_k\left(1-\alpha\right)\sqrt{x_{Dw}}\right) \quad \text{.....(D-6)}$$
$$c_2 = \alpha\exp\left(\varepsilon_k\left(1-\alpha\right)\sqrt{x_{Dw}}\right)$$

Finally, the integral in eq. D-3 is equal to

$$\varepsilon_k \int_{x_{Dw}}^{x_D} \frac{C\left(x_D\right)Y\left(x_D\right)}{x_D\sqrt{x_D}}\,dx_D = c_1 \int_{\exp\left[-\varepsilon_k\left(1-\alpha\right)\sqrt{x_{Dw}}\right]}^{\exp\left[-\varepsilon_k\left(1-\alpha\right)\sqrt{x_D}\right]} \frac{1}{\left(1-c_2u\right)\ln^2\left(u\right)}\,du$$

$$+c_1\alpha\exp\left[\varepsilon_k\left(1-\alpha\right)\sqrt{x_{Dw}}\right] \int_{\exp\left[-\varepsilon_k\left(1-\alpha\right)\sqrt{x_{Dw}}\right]}^{\exp\left[-\varepsilon_k\left(1-\alpha\right)\sqrt{x_D}\right]} \frac{u}{\left(1-c_2u\right)^2\ln^2\left(u\right)}\,du \text{ .(D-7)}$$

Substitution of eq. D-7 into eq. D-3 provides with explicit formula for the impedance slope *m*.

Figure Captions

Fig. 1—Schema for barium sulphate deposition in the well vicinity due to produced water re-injection.

Fig. 2—Concentration profiles behind the injection water front on the plane (x_D,t_D).

Fig. 3—Profiles for Ba^{2+} concentration for different kinetics numbers: ε_k = 0.94 ; 4.68 ; 18.72 ; 46.8 (curves 1,2,3 and 4, respectively).

Fig. 4a—Profiles for deposited concentration: for different times: $t_D = 5*10^5$; 10^6; $5*10^6$; $1.1*10^7$ and ε_k= 18.72

Fig. 4b—Profiles for deposited concentration: curve 1: ε_k = 3.7, α = 0.01; curve 2: ε_k = 3.7, α = 0.1; curve 3: ε_k = 18.72, α = 0.01; curve 4: ε_k = 18.72, α = 0.1.

Fig. 5—Function $M(x_D)$ achieves the asymptotic value at the distance from the well that equals 1.3 and 2.2 well radius. Curves 1, 2, 3 and 4 corresponds to ε_k = 18.74 and α= 0.02; ε_k = 18.74 and α = 0.2, ε_k = 4.7 and α = 0.02, ε_k = 4.7 and α = 0.2, respectively.

Fig. 6—Effect of kinetics number on formation damage zone radius for different concentration ratios.

Fig. 7—Sensitivity analysis of impedance constant M:
a) M versus kinetics number for various concentration ratios α;
b) Effect of concentration ratio a on impedance constant M for various ε_k.

Fig. 8a—Effect of kinetics coefficient on injectivity decline (β = 100, r_d = 0.2 m, R_c = 500 m): impedance growth for four different values of kinetics number: ε_k = 0.94 ; 4.68 ; 18.72 ; 46.8.

Fig. 8b—Effect of kinetics coefficient on injectivity decline (β = 100, r_d = 0.2 m, R_c = 500 m): injectivity decline for different values of kinetics number;

Fig. 8c—Effect of kinetics coefficient on injectivity decline (β = 100, r_d = 0.2 m, R_c = 500 m): decline of injectivity index versus real time (months).

Fig. 9a—Injectivity index versus time: curves 1, 2, 3 and 4 correspond to different concentration ratios, barium concentrations are 1.1, 5.0, 10.0 and 20.0 ppm: time t_D in pore volumes of the reservoir pattern;

Fig. 9b—Injectivity index versus time: curves 1, 2, 3 and 4 correspond to different concentration ratios, barium concentrations are 1.1, 5.0, 10.0 and 20.0 ppm: time t in months.

Fig. 10—Effect of produced water fraction in the injected fluid on barium concentration profile: $C_1(x_D)$ - SW : PW = 4 : 1; $C_2(x_D)$ - SW : PW = 1 : 1; $C_3(x_D)$- SW : PW = 1 : 4.

Fig. 11a—Barium sulphate deposition profile for different fractions of produced water in the injected fluid: $S1u(x_D)$: SW : PW = 4 : 1 (ε_k = 13.92, α= 0.005); $S2u(x_D)$: SW : PW = 1 : 1 (ε_k = 8.7, α = 0.02); $S3u(x_D)$: SW : PW = 1 : 4 (ε_k = 3.48, α = 0.08);

Fig. 11b—Barium sulphate deposition profile for different fractions of produced water in the injected fluid: $S1(x_D)$: SW : PW = 4 : 1; $S2(x_D)$: SW : PW = 1 : 1; $S3(x_D)$: SW : PW = 1 : 4 (at t_D = 1 p.v.i.)

Fig. 12—Function $M(x_D)$ achieves the asymptotic value at the distance from the well that equals 1.45, 1.69 and 2.59 well radius, respectively.

Fig. 13—Sensitivity of impedance constant M versus fraction N.

Fig. 14—Sensitivity of impedance slope m versus fraction N.

Fig. 15a—Effect of different fractions of produced water in the injected fluid on injectivity decline: impedance growth for three different fractions: (SW : PW = 4 : 1); (SW : PW = 1 : 1); (SW : PW = 1 : 4).

Fig. 15b—Effect of different fractions of produced water in the injected fluid on injectivity decline: injectivity decline for different fractions.

Fig. 15c—Effect of different fractions of produced water in the injected fluid on injectivity decline: decline of injectivity index versus real time (months) R_c = 500m; r_w = 0.15m; β = 100; Q = 55000 BBL/day; h = 152.4m; ϕ= 0.356.

Fig. 16a—Maximum barium concentration in injected water causing given injectivity index decline: m = 1 (causing two times injectivity decline during 1 pore volume injected) and m = 4 (causing five times injectivity decline during 1 pore volume injected): versus kinetics coefficient λ.

Fig. 16b—Maximum barium concentration in injected water causing given injectivity index decline: m = 1 (causing two times injectivity decline during 1 pore volume injected) and m = 4 (causing five times injectivity decline during 1 pore volume injected): versus kinetics number ε_k.

TABLE 1—CHEMICAL KINETICS AND FORMATION DAMAGE COEFFICIENTS AS OBTAINED FROM DIFFERENT COREFLOOD TESTS

Coreflood Test	Kinetics Coefficient λ, $(M*m)^{-1}$	Formation Damage Coefficient β
Lopes Jr., 2002[16,17]	3003 – 3951	-
Todd et al., 1992[15]		
BSS0	23720 – 42200	46 – 79
BSS1	5540 – 9310	27 – 43
BSS2	1553 – 2760	43 – 74
Water 1	922 – 1578	60 – 97
Wat et al., 1992[14]	798 – 963	-

TABLE 2A—BARIUM CONCENTRATION IN INJECTED WATER CAUSING TWO TIMES INJECTIVITY DECLINE DURING GIVEN TIME (FIELD CASE, NORTH SEA, UK)

t_D, p.v.i.	T, months	m	max C_{Ba}^{2+}, ppm
0,010	1	1	3,25
0,037	3	1	1,10
0,074	6	1	0,55
0,150	12	1	0,27
0,440	36	1	0,09
1	82	1	0,04

TABLE 2B—BARIUM CONCENTRATION IN INJECTED WATER CAUSING FIVE TIMES INJECTIVITY DECLINE DURING GIVEN TIME (FIELD CASE, NORTH SEA, UK)

t_D, p.v.i.	T, months	m	max C_{Ba}^{2+}, ppm
0,010	1	4	15.90
0,037	3	4	4.30
0,074	6	4	2.15
0,150	12	4	1.06
0,440	36	4	0.361
1	82	4	0.159

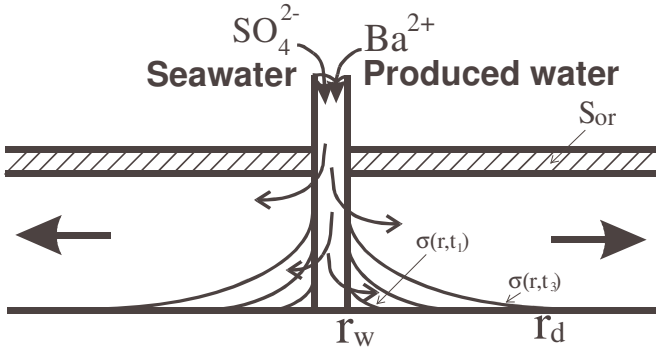

Fig. 1—Schema for barium sulphate deposition in the well vicinity due to produced water re-injection.

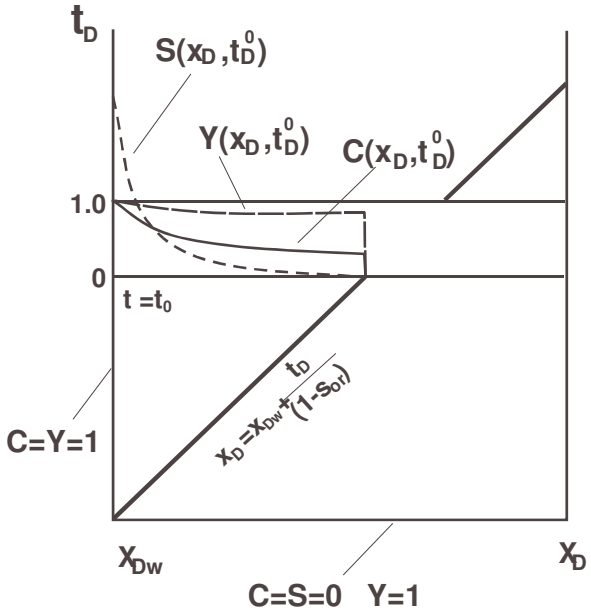

Fig. 2—Concentration profiles behind the injection water front on the plane (x_D,t_D).

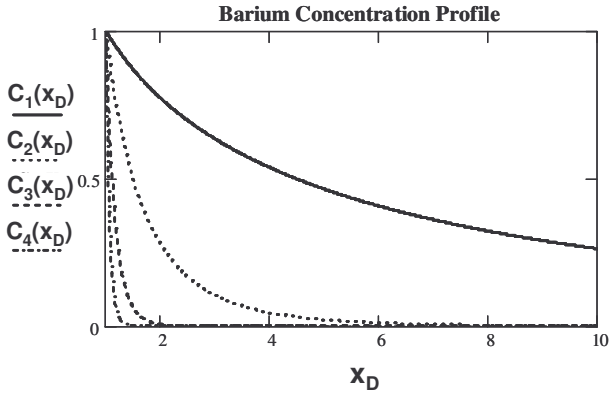

Fig. 3—Profiles for Ba^{2+} concentration for different kinetics numbers: ε_k = 0.94 ; 4.68 ; 18.72 ; 46.8 (curves 1,2,3 and 4, respectively).

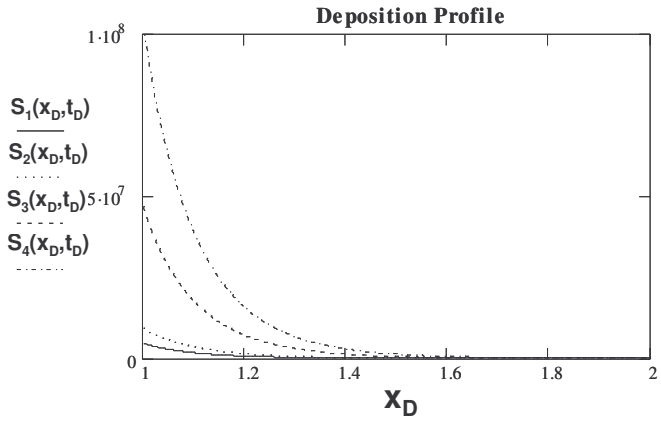

4a)

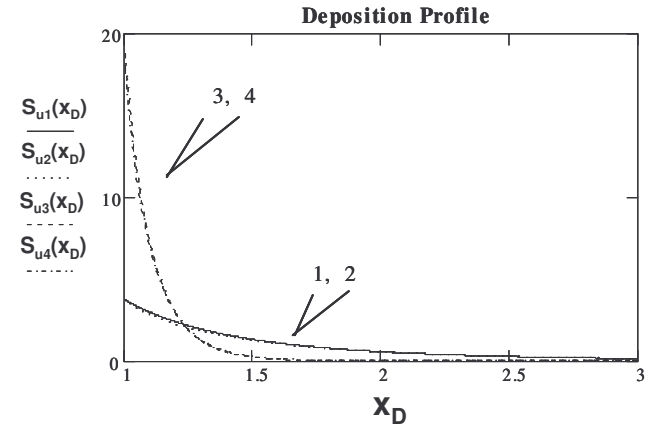

4b)

Fig. 4—Profiles for deposited concentration:
a) for different times: t_D = 5*105; 106; 5*106; 1.1*107 and ε_k = 18.72;
b) curve 1: ε_k = 3.7, α = 0.01; curve 2: ε_k = 3.7, α = 0.1; curve 3: ε_k = 18.72, α = 0.01; curve 4: ε_k = 18.72, α = 0.1.

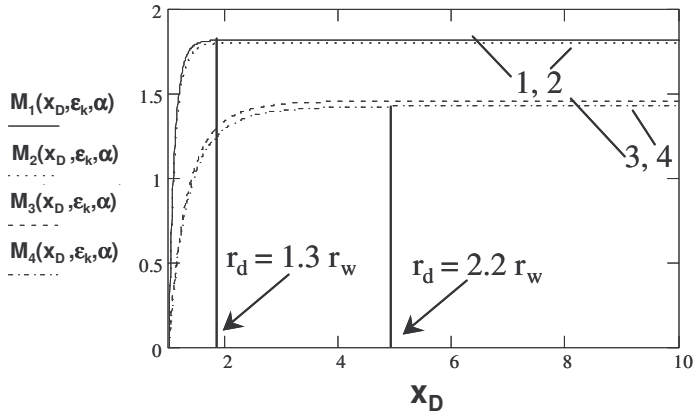

Fig. 5—Function $M(x_D)$ achieves the asymptotic value at the distance from the well that equals 1.3 and 2.2 well radius $\tilde{s}$

Curves 1, 2, 3 and 4 corresponds to ε_k = 18.74 and α = 0.02; ε_k = 18.74 and α = 0.2, ε_k = 4.7 and α = 0.02, ε_k = 4.7 and α = 0.2, respectively.

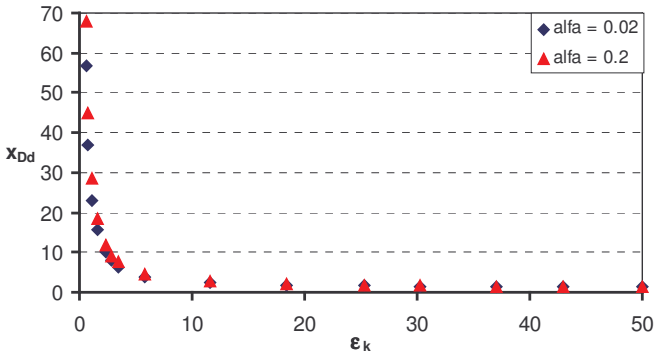

Fig. 6—Effect of kinetics number on formation damage zone radius for different concentration ratios.

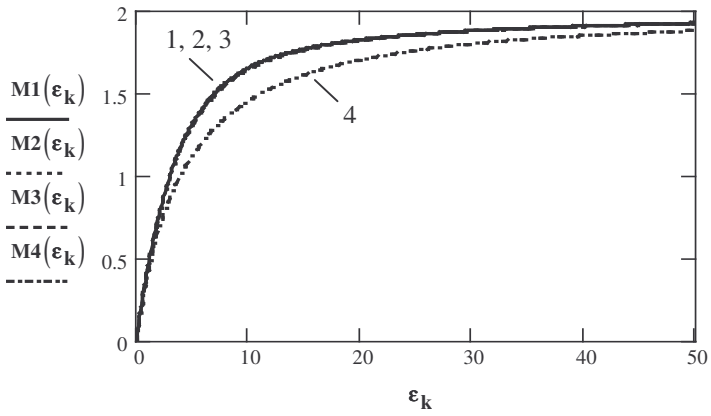

7a)

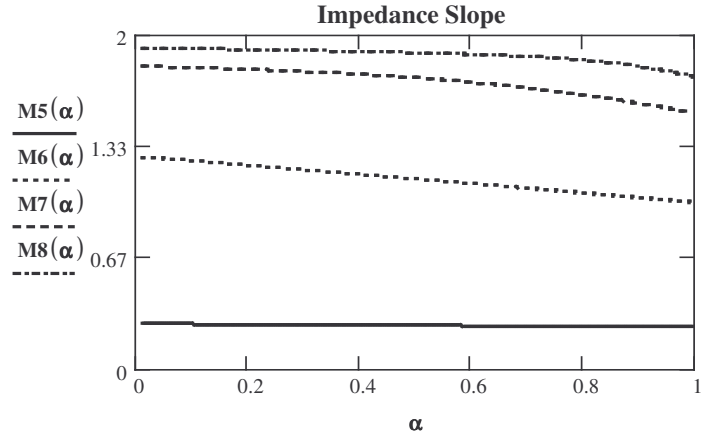

7b)

Fig. 7—Sensitivity analysis of impedance constant *M*:
a) *M* versus kinetics number for various concentration ratios α;
b) Effect of concentration ratio α on impedance constant *M* for various ε_k.

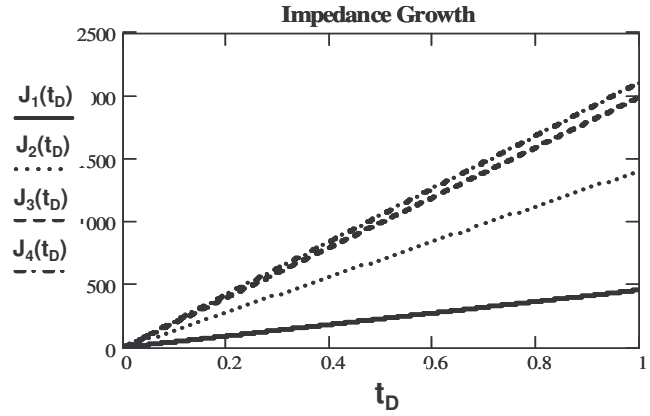

8a)

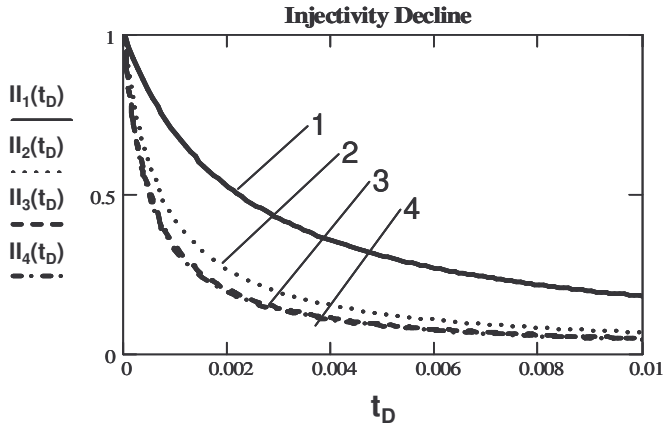

8b)

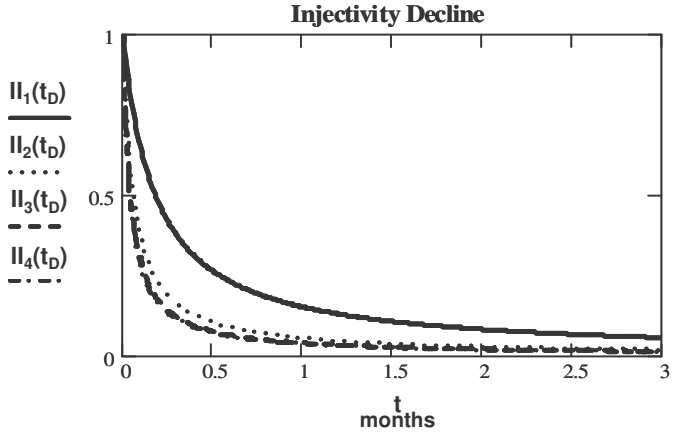

8c)

Fig. 8—Effect of kinetics coefficient on injectivity decline (β = 100, r_d = 0.2 m, R_c = 500 m):
a) impedance growth for four different values of kinetics number: ε_k = 0.94 ; 4.68 ; 18.72 ; 46.8;
b) injectivity decline for different values of kinetics number;
c) decline of injectivity index versus real time (months).

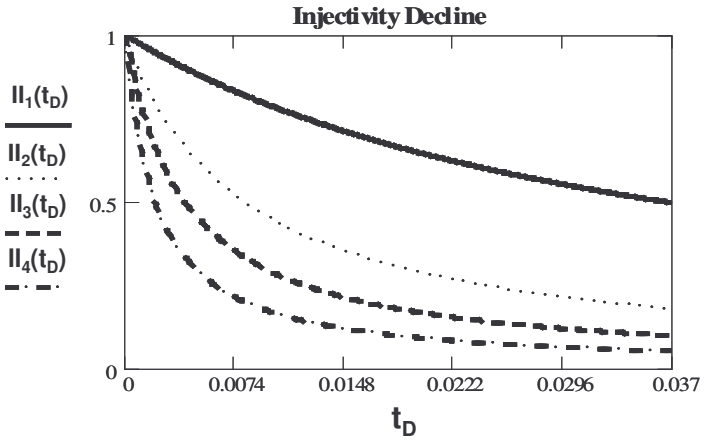

9a)

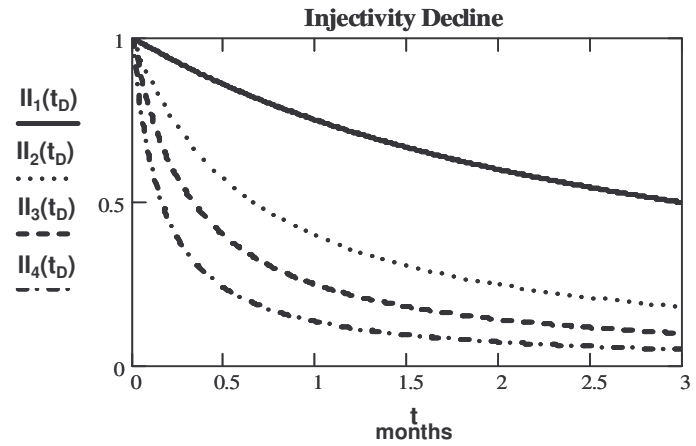

9b)

Fig. 9—Injectivity index versus time: curves 1, 2, 3 and 4 correspond to different concentration ratios, barium concentrations are 1.1, 5.0, 10.0 and 20.0 ppm:
a) time t_D in pore volumes of the reservoir pattern;
b) time t in months.

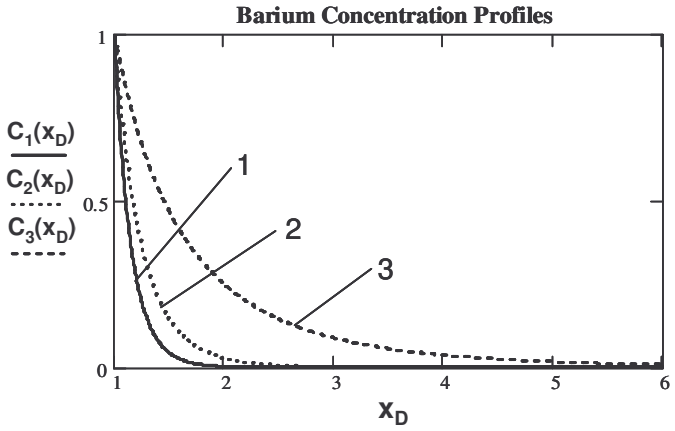

Fig. 10—Effect of produced water fraction in the injected fluid on barium concentration profile: *$C_1(x_D)$ - SW : PW = 4 : 1*; *$C_2(x_D)$ - SW : PW = 1 : 1*; *$C_3(x_D)$- SW : PW = 1 : 4*.

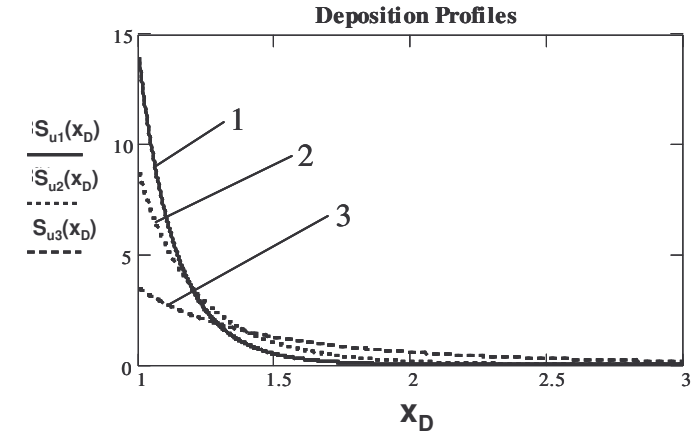

11a)

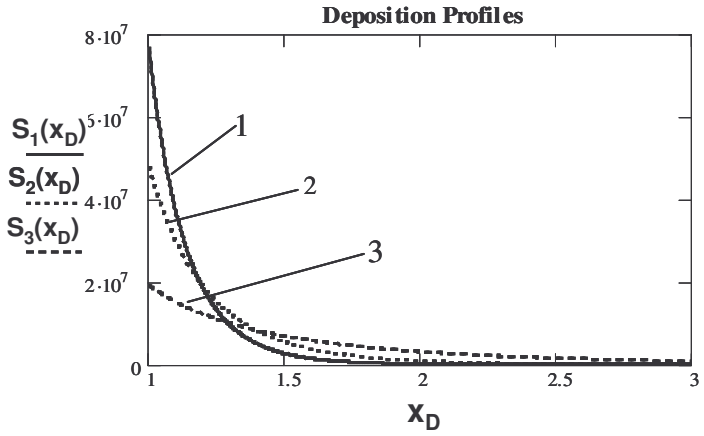

11b)

Fig. 11—Barium sulphate deposition profile for different fractions of produced water in the injected fluid:
a) ***S1$_u$(x$_D$): SW : PW = 4 : 1*** **(**ε_k **= 13.92,** α **= 0.005);** ***S2$_u$(x$_D$): SW : PW = 1 : 1*** **(**ε_k ***= 8.7,*** α ***= 0.02*****);** ***S3$_u$(x$_D$): SW : PW = 1 : 4*** **(**ε_k ***= 3.48,*** α ***= 0.08*****);**
b) ***S1(x$_D$): SW : PW = 4 : 1*****;** ***S2(x$_D$): SW : PW = 1 : 1*****;** ***S3(x$_D$): SW : PW = 1 : 4*** **(at** t_D **= 1 p.v.i.).**

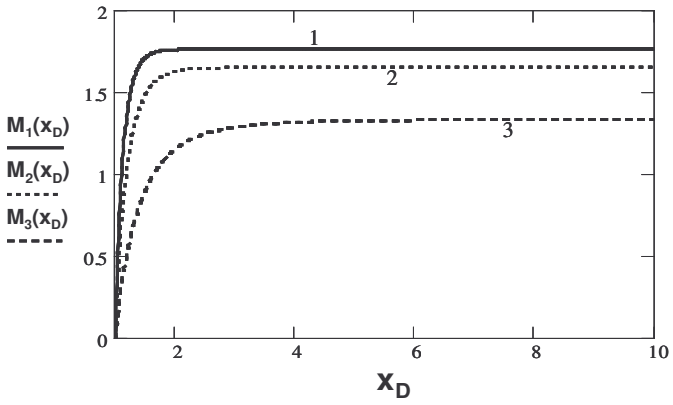

Fig. 12—Function *M(x_D)* achieves the asymptotic value at the distance from the well that equals 1.45, 1.69 and 2.59 well radius, respectively.

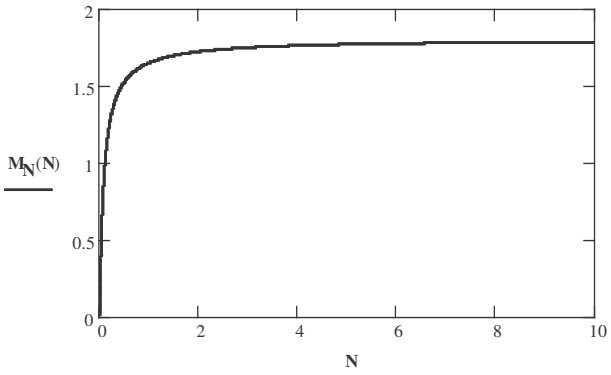

Fig. 13—Sensitivity of impedance constant *M* versus fraction *N*.

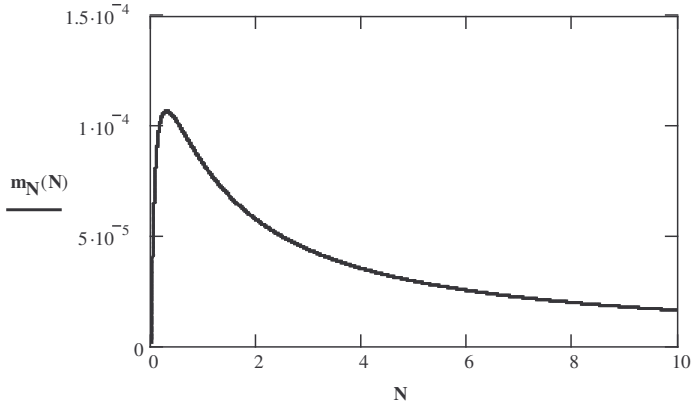

Fig. 14—Sensitivity of impedance slope *m* versus fraction *N*.

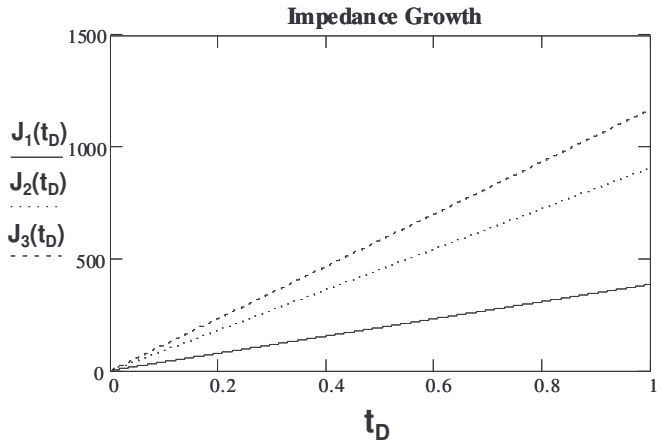

15a)

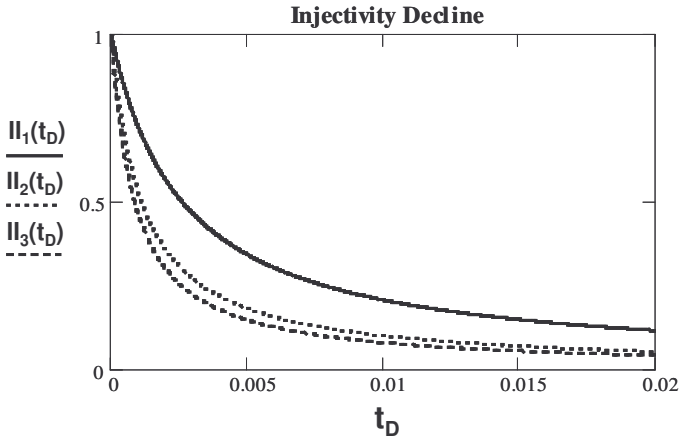

15b)

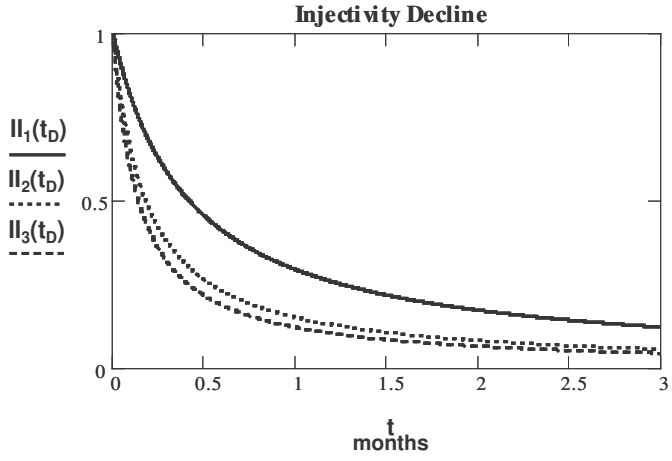

15c)

Fig. 15—Effect of different fractions of produced water in the injected fluid on injectivity decline:
a) impedance growth for three different fractions: (*SW : PW = 4 : 1*); (*SW : PW = 1 : 1*); (*SW : PW = 1 : 4*);
b) injectivity decline for different fractions;
c) decline of injectivity index versus real time (months)
***R_c = 500m*; *r_w = 0.15m*; *β = 100*; *Q = 55000 BBL/day*; *h = 152.4m*; *ϕ= 0.356*.**

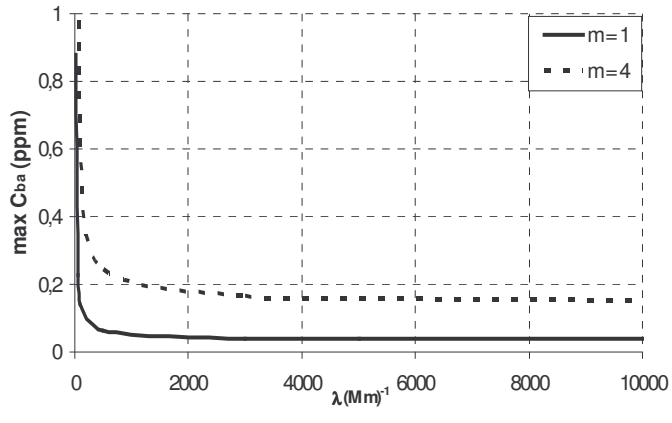

16a)

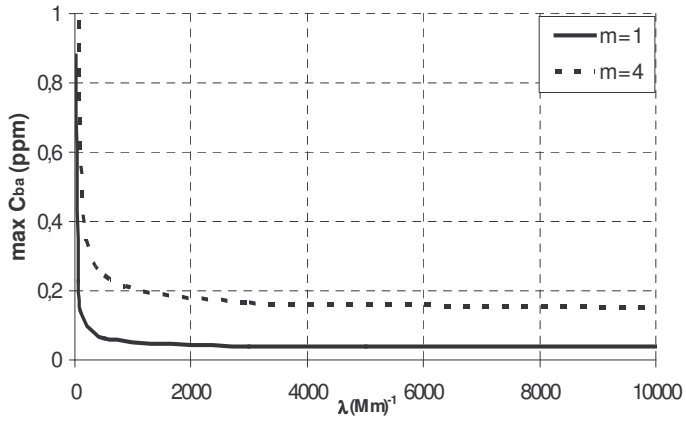

16b)

Fig. 16—Maximum barium concentration in injected water causing given injectivity index decline: m = 1 (causing two times injectivity decline during 1 pore volume injected) and m = 4 (causing five times injectivity decline during 1 pore volume injected):

a) versus kinetics coefficient λ;
b) versus kinetics number ε_k.